

RESEARCH

Open Access



# Enhancing Quality Control in the Mix Design of High-Strength Concrete Using a Capacity-Based Approach

Dhiman Basu<sup>1\*</sup>, Sheikh Mayesser Mushtaq<sup>1</sup>, Shivani Sharma<sup>1</sup> and Sandesh Tripathi<sup>1</sup>

## Abstract

The mix design of concrete is an important aspect that affects its strength and durability. This paper aims to revisit the existing mix design method given in IS 10262:2019 through a capacity-based approach. The approach involves identifying the possible failure modes in concrete and eliminating the undesirable ones leading to significant reduction in dispersion. This is accomplished by utilizing coarse aggregates that meet a specific minimum strength requirement or threshold (e.g., ~77 MPa for M95 grade of concrete), which is determined through a priori estimating the cohesion and friction angle of the concrete. The methodology to estimate the cohesion and friction angle from a single unconfined compression test is proposed based on the Mohr–Coulomb theory and using the orientation of failure plane of fractured specimen as a supplemental information from the same experiment. This paper also offers a simple and approximate test procedure to estimate the aggregate's compressive strength (~106 MPa in this mix design) reasonably which is essential for the capacity-based mix design. An experimental programme is also carried out to design the concrete mix using the proposed capacity-based approach. The results indicate that M95 concrete is achieved with a low standard deviation and coefficient of variation (~3%), falling in class of excellent quality control as per ACI 214R-11. This quality control is crucial in seismic structural design as variations in concrete strength is likely to negate the underlying principle of strong column–weak beam philosophy resulting in the triggering of undesirable shear modes of failure.

**Keywords** Mix design, High-strength concrete, Capacity-based approach, Quality control, Cohesion and friction angle

## 1 Introduction

Normal strength concrete (NSC) is typically defined with the maximum 28-day compressive strength of approximately 40 MPa, and the associated mix design procedure does not require any admixtures. Several significant drawbacks, including low tensile strength, high brittleness, low specific strength and low energy absorption

during failure are recognized in NSC (Sohail et al., 2018). Mix design procedures have now advanced significantly with an emphasis on developing high-strength concrete (HSC), which is believed to offer advantages such as reduced cross-sectional area and weight, and thereby enhancing its seismic performance. This is typically designated as the concrete with 28-day compressive strength exceeding 60 or 65 MPa (IS 10262, 2019; SP228, 2005). HSC is often designed by reducing the nominal size of the coarse aggregate to as low as 10 mm when targeting a strength in the order of 60 MPa, or even without using coarse aggregate when targeting strengths of 90 MPa or higher. Supplementary cementitious materials (SCMs) like silica fume (SF), metakaolin (MK), fly ash, ground

Journal information: ISSN 1976-0485 / eISSN 2234-1315.

\*Correspondence:

Dhiman Basu  
dbasu@iitgn.ac.in

<sup>1</sup> Department of Civil Engineering, Indian Institute of Technology, Gandhinagar, India

granulated blast furnace slag, etc., are often added as partial replacement of cement to reduce the porosity and improve the interfacial transition zone (ITZ). Superplasticizers are included to maintain the desired workability for a specified duration with or without a retarder.

Strength of the hardened concrete can be improved in several ways, for example, using partial replacement of ordinary Portland cement (OPC) by mineral and chemical admixtures (Lämmlein et al., 2019; Zhang et al., 2017), employing diverse types of aggregates (Jóźwiak-Niedźwiedzka, 2005; Ma et al., 2019), addition of fibres (Shen et al., 2020; Smarzewski, 2019; Xu et al., 2019; Yew et al., 2015) as well as adopting different curing techniques (Jiang et al., 2014; Tan & Zhu, 2017). Some of them were reported to have positive effects on strength enhancement of high-performance concrete (HPC), while others had shown negative effects beyond a threshold. This variability may be attributed to several factors including the suitability of the selected raw materials including the admixtures and SCMs. Conflicting inferences were also reported about the possible synergistic effects while using the ternary blend (Dushimimana et al., 2021).

MK and SF are two frequently utilized SCMs in high-strength concrete and Table S1 in the supplement summarizes several studies that investigated the effects of MK, SF, and their combinations on cementitious systems. The optimal proportion for enhancing concrete properties was typically reported as 10–15% by weight of cement when utilized as a binary blend in the mixture. Using higher proportions might result in the loss of strength (Dushimimana et al., 2021). Several studies reported higher compressive strength while using SF in binary blend when compared with MK (Bilal et al., 2021; Chen et al., 2020; Güneyisi et al., 2012), whereas several other studies reported otherwise (Chu & Kwan, 2019; Chu et al., 2021; Güneyisi et al., 2010, 2012; Poon et al., 2006; Shah & Scott, 2021). Simultaneous use of SF and MK in HSC hints around a possible synergistic effect when compared with the binary blending. Nevertheless, SF has traditionally been a preferred choice (over MK) owing to its silica content of at least 85% and ultra-fine particle size, which not only improves strength but also enhances durability by reducing porosity and enhancing the quality of transition zones (Chu et al., 2021). Other materials like ground granulated blast furnace slag (GGBS) (Huynh et al., 2022; Piro et al., 2022), rice husk ash (Safiuddin et al., 2010; Van et al., 2014), calcined clay (Mo et al., 2022; Rossetti et al., 2021), limestone (Mo et al., 2022; Rossetti et al., 2021), etc., are also used as SCMs in high-strength concrete.

Further, the aggregate strength should not impede the required strength development in HSC (Dushimimana

et al., 2021); Shin et al., 2019). Zhang and Islam (2012) inferred crushing of aggregate regardless of the strength surrounding matrix with the following observations: (i) cracks propagated through the coarse aggregates limiting the strength of the concrete to 70 MPa, and (ii) the weaker coarse aggregates reached their limiting strength and in turn, becoming the weakest link. Similar observations also hold in lightweight aggregate (LWA) concrete (Ahmad & Chen, 2019; Bogas & Gomes, 2013; Kayali, 2008; Nepomuceno et al., 2018; Zhou et al., 1995). IS 10262 (2019) also recommends crushed stone aggregates with a crushing value of not more than 22% in HSC. Shin et al., (2019) recommends aggregate strength greater than the matrix strength in HSC. Hence, ensuring sufficient strength of coarse aggregate is imperative in the mix design of HSC.

Based on the limited review presented above, the current concrete mix design frameworks lack proper control over the potential failure modes despite some recommendations on the quality control of the raw materials. Uncertainty in the prediction of concrete strength can alter the sequence of plastic hinge formation during a seismic event, potentially leading to the undesirable mode of brittle shear failure. This paper aims to propose a methodology for better quality control by a) suppressing (postponing) the undesirable aggregate failure mode and b) preponing the mortar failure mode. This is because the dispersion of the aggregate phase strength is envisioned to be relatively higher than that of the mortar phase as (i) aggregate is procured from natural sources that involves aleatory and epistemic uncertainties; (ii) scope of reducing the epistemic uncertainty is nearly zero as it is used without any processing during the mix design; (iii) strength of mortar can be controlled by deciding the relative proportion of the constituents and hence, the epistemic uncertainty in mortar phase strength can be reduced significantly. Therefore, targeting weaker mortar–stronger aggregate is likely to result in the minimum dispersion of compressive strength of HSC. Quantitative assessment of aggregate strength relevant to the concrete mix design is also proposed in an approximate strength. Assessment of the threshold aggregate strength to ensure mortar failure requires estimation of Mohr–Coulomb parameters of concrete. Further, concrete being a heterogeneous material leads to its property variations across different cube samples even within the same batch. As a result,  $c - \phi$  values estimated using different concrete cube specimens are likely to be affected by the sample-to-sample variability. This paper proposes a framework for the estimation of these parameters using one single unconfined compression test, which is something unique when compared with the prior art. However, absence of ITZ is a crucial assumption in this framework, which

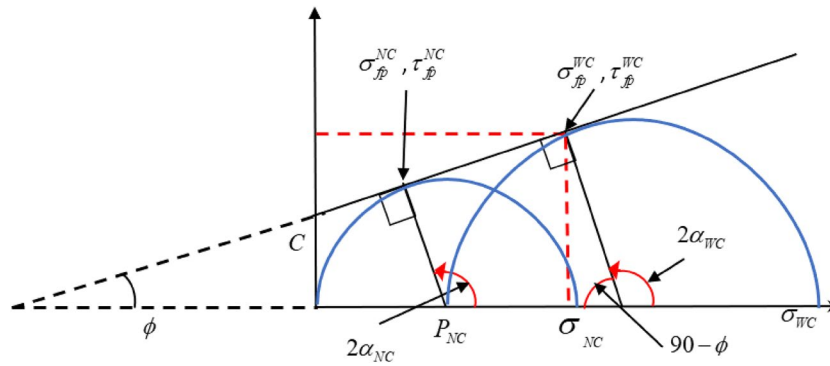


**Fig. 1** Schematic representation of failure envelopes for Mohr–Coulomb's theory

may not necessarily hold even in HSC. Nonetheless, the utilization of supplementary cementitious materials and a low water-to-cement ratio in HSC may significantly improve the ITZ formation and thereby enabling the application of proposed framework. This paper explores SF and MK in ternary blend for the overall performance. Finally, the mix design method recommended in IS 10262 (2019), is revisited in this paper through a perspective of capacity-based approach resulting in some concrete with low standard deviation in compressive strength and thereby enhancement in quality control.

### 2 Parameters c-phi Using a Single Unconfined Compression Test

Assuming that a homogeneous and isotropic material that conforms to the Mohr–Coulomb failure theory, consider two uniaxial compression tests, one without any confinement and the other at a confining pressure  $P_{NC}$ . Mohr–Coulomb failure envelopes along with the Mohr circles are shown in Fig. 1. The confined compressive strength ( $\sigma_{WC}$ ) can be expressed as:

$$\sigma_{WC} = P_{NC} \left( \frac{1 + \sin \phi}{1 - \sin \phi} \right) + 2c \left( \frac{\cos \phi}{1 - \sin \phi} \right). \tag{1}$$

Here,  $c - \phi$  denote the cohesion and angle of internal friction. Associated normal and shear stresses at the failure plane are given by:

$$\begin{aligned} \sigma_{fp}^{WC} &= \frac{\sigma_{WC}}{2} (1 - \sin \phi) + \frac{P_{NC}}{2} (1 + \sin \phi), \\ \tau_{fp}^{WC} &= \left( \frac{\sigma_{WC} - P_{NC}}{2} \right) \cos \phi. \end{aligned} \tag{2}$$

Next, the unconfined compression test is considered and let  $\sigma_{NC}$  be the unconfined compressive strength. Associated normal and shear stresses at the failure plane are given by:

$$\begin{aligned} \sigma_{fp}^{NC} &= \frac{\sigma_{NC}}{2} (1 - \sin \phi), \\ \tau_{fp}^{NC} &= \frac{\sigma_{NC}}{2} \cos \phi. \end{aligned} \tag{3}$$

Utilizing both the results, friction angle may be expressed as:

$$\tan \phi = \frac{\tau_{fp}^{WC} - \tau_{fp}^{NC}}{\sigma_{fp}^{WC} - \sigma_{fp}^{NC}} \tag{4}$$

Utilizing Eq. (2) and Eq. (3) in Eq. (4), one may write

$$\begin{aligned} \frac{\sigma_{WC} - \sigma_{NC}}{P_{NC}} &= \frac{1 + \sin \phi}{1 - \sin \phi}, \\ \phi &= 2 \tan^{-1} \left[ \sqrt{\frac{\sigma_{WC} - \sigma_{NC}}{P_{NC}}} \right] - \frac{\pi}{2}. \end{aligned} \tag{5}$$

Using the friction angle from Eq. (5), the cohesion can be estimated using the unconfined compressive strength as follows:

$$c = \tau_{fp}^{NC} - \sigma_{fp}^{NC} \tan \phi = \frac{\sigma_{NC}}{2} \left( \frac{1 - \sin \phi}{\cos \phi} \right). \tag{6}$$

First part of Eq. (5) may be rearranged of the form

$$\frac{1 - \sin \phi}{\cos \phi} = \sqrt{\frac{P_{NC}}{\sigma_{WC} - \sigma_{NC}}}. \tag{7}$$

Finally, substituting Eq. (7) in Eq. (6), one may express the cohesion as:

$$c = \frac{\sigma_{NC}}{2} \left( \frac{1 - \sin \phi}{\cos \phi} \right) = \frac{\sigma_{NC}}{2} \sqrt{\frac{P_{NC}}{\sigma_{WC} - \sigma_{NC}}}. \tag{8}$$

If one unconfined and one confined compression tests are performed, second part of Eq. (8) may be used for the computation of cohesion. However, the first part of Eq. (8) may be used if it is possible to estimate the

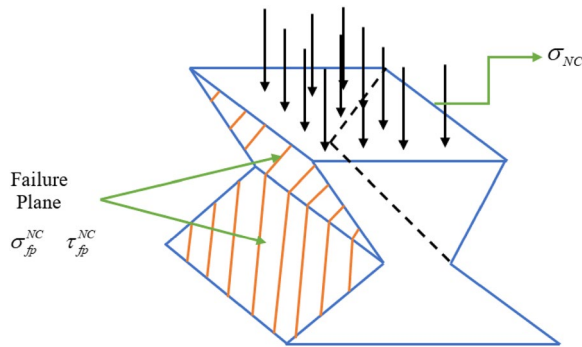


**Fig. 2** Representation of fractured cube specimen with exposed failure plane

friction angle from the unconfined compression test. As evident from Fig. 1, the orientation of the failure plane is not influenced by the presence of confining pressure, i.e.  $\alpha_{WC} = \alpha_{NC}$ . Here, the angle  $\alpha$  is measured in counterclockwise direction with respect to the major principal plane, which is horizontal in a typical compression test. Therefore, the friction angle can be estimated after observing the orientation  $\alpha_{NC}$  of the fractured unconfined test sample. Fig. 2 presents the sample illustration for a typical cube specimen and one may write

$$\phi = 2\alpha_{NC} - \frac{\pi}{2} \quad \left( \frac{\pi}{4} \leq \alpha_{NC} \leq \frac{\pi}{2} \right). \quad (9)$$

Note that orientation of the failure plane with respect to both top and bottom horizontal planes are same but opposite in sense. It is proposed to consider average of these two orientations (without sign) when extrapolating the unconfined compression test results for a material that does not strictly follow Mohr–Coulomb theory. Therefore, it may be possible to determine  $c - \phi$  using one unconfined compression test by i) noting the failure load / stress; and ii) approximately identifying the orientation of failure plane with respect to the horizontal plane. Further details on this procedure are reported elsewhere (Sharma, 2024).

### 2.1 At Failure of Unconfined Compression Test

Once  $c - \phi$  are estimated, normal and shear stresses at the failure plane may be calculated using Eq. (3). Further, the shear strength at the failure plane is also given by:

$$\tau_{fp}^{NC} = c + \sigma_{fp}^{NC} \tan \phi. \quad (10)$$

In other words, when the load is progressively increased on the specimen, shear stress at the failure plane will reach to  $c$  at some point of time denoting the breaking of cohesion. At this stage,  $\tan \phi$  acts as the friction coefficient on the sliding interface until the shear strength at

the interface / failure plane, i.e. the compressive strength on the horizontal plane is reached. Substituting the first part of Eq. (8) and Eq. (3) into Eq. (10), one may show the shear strength is given by the second part of Eq. (3). This is readily evident from the Mohr–Coulomb failure envelop also (Fig. 3).

### 2.2 Comparison at Loss of Cohesion and at Failure of Unconfined Compression Test

Fig. 3 enables the comparison of two states, namely, (i) loss of cohesion and (ii) failure. Let  $\sigma_{CH}$  be the applied vertical stress at which cohesion is lost on the failure plane and in that case,

$$c = \frac{\sigma_{CH}}{2} \cos \phi. \quad (11)$$

The associated normal stress on the failure plane is given by:

$$\sigma_{fp,CH}^{NC} = \frac{\sigma_{CH}}{2} (1 - \sin \phi). \quad (12)$$

Further, using Mohr–Coulomb envelop, the shear strength (at failure) is given as:

$$\tau_{fp}^{NC} = \sigma_{fp}^{NC} \tan \phi + c = \frac{\sigma_{NC}}{2} \cos \phi. \quad (13)$$

Now, equating Eq. (11) and first part of Eq. (8), one may write

$$\frac{\sigma_{CH}}{\sigma_{NC}} = \frac{1 - \sin \phi}{\cos^2 \phi}. \quad (14)$$

The required step-by-step procedure may be summarized as follows:

- (1) Observe the compressive strength  $\sigma_{NC}$ ; (2) observe the failure plane and identify  $\alpha_{NC}$ ; (3) compute the shear angle  $\phi$  using Eq. (9); (4) compute the cohesion  $c$  using

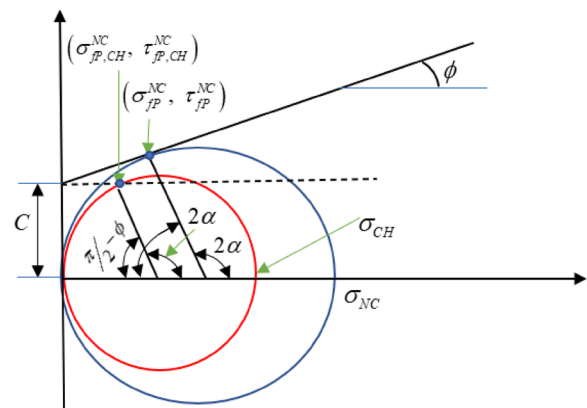


**Fig. 3** Estimation of  $C-\phi$  for cube specimen using one unconfined test

$\sigma_{NC}$  and  $\phi$  in the first part of Eq. (8); (5) compute the vertical stress at which the cohesion is lost,  $\sigma_{CH}$ , using Eq. (14).

The framework presented above applies to a homogeneous and isotropic material that conform to Mohr–Coulomb failure theory. The same procedure may be extended to mortar and concrete cube (provided ITZ is absent). It may also be extended to coarse aggregates if it is possible to perform compression test on a single specimen of aggregate. Since the aggregate is brittle in nature, friction angle ( $\phi_{agg}$ ) may however be approximated as zero and the entire shear strength ( $\tau_{agg}$ ) is given by its cohesion,  $c_{agg}$ :

$$\tau_{agg} = \frac{\sigma_{NC}^{agg}}{2} = c_{agg}, \quad (15)$$

$$\phi_{agg} = 0.$$

Here,  $\sigma_{NC}^{agg}$  denotes the observed compressive strength. In such a case, confinement does not improve the shear strength (Fig. 4).

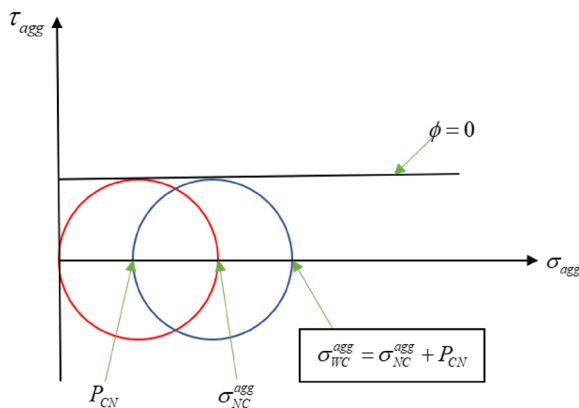


**Fig. 4** Schematic representation of aggregate confined by hardened mortar

### 3 Capacity-Based Mix Design for High-Strength Concrete

Owing to the random distribution and orientation of the coarse aggregates, the resulting load transfer (prior to the loss of cohesion) may be considered as direct compression or pure shear or a combination of the two (Fig. 5). Five possible failure modes may exist, namely, compression- and shear-failure of coarse aggregate- and mortar-phase and interfacial transition zone (ITZ). Clubbing these modes of failure, concrete is considered as three-phased, namely, aggregate phase, mortar phase and ITZ. The aim is to achieve the lowest possible dispersion, given the target strength, and the principle proposed for that is to ensure one failure mode with the highest control.

ITZ is primarily formed due to two effects: first, the formation of water-filled spaces around the aggregates in the fresh mix; and second, the “wall effect” which prevents effective filling of the space adjacent to coarse aggregates. As a result, the space around the aggregates is ineffectively filled with hydration products and becomes less dense when compared with the bulk paste (i.e. mortar phase). However, in case of HSC, these factors become less significant due to the relatively little difference in the microstructural gradient near coarse aggregate in comparison to the bulk paste. This is typically the case in HSC with w/c ratio less than 0.4. Reduced nominal size of the coarse aggregates in HSC also weakens the significance of the “wall effect”. Adding mineral admixtures such as silica fume (SF), metakaolin (MK), etc., also results in a denser and homogenous structure near the coarse aggregate surface, similar to that of the bulk paste/mortar phase. Given this understanding, ITZ is not considered in this paper, and the capacity-based principle is hypothesized solely on the existence of mortar and aggregate phases.

Any of these two possible candidates can be set to govern the compressive strength of concrete by carefully selecting the aggregate and designing the mortar paste.

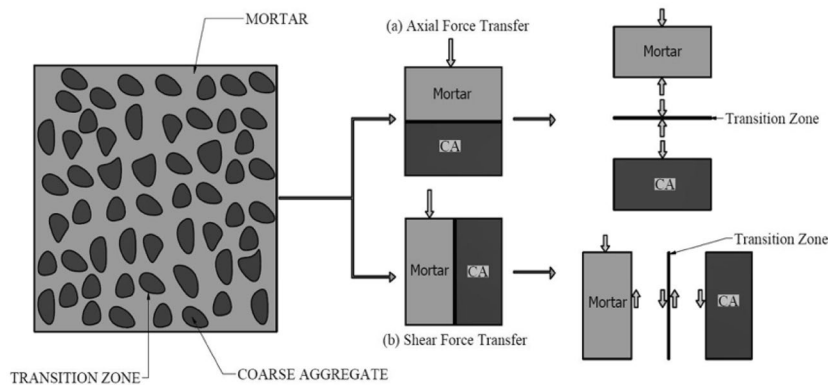


**Fig. 5** Load transfer mechanism in concrete matrix

The resulting dispersion in the compressive strength of concrete is contingent on that of both the aggregate and mortar phase strength. However, the primary contributor is the dispersion of the lower strength that controls the failure of concrete. For example, if the aggregate is weaker than mortar, the dispersion of compressive strength of concrete will be governed by that of the aggregate phase strength and vice-versa.

Dispersion of the aggregate phase strength is expected to be relatively higher than that of the mortar phase due to i) various uncertainties in the natural sources and ii) the limited scope of reducing the epistemic uncertainty during mix design (as it is used without any processing). However, the strength of the mortar can be controlled by deciding the relative proportion of the constituents, which significantly reduces the associated epistemic uncertainty. Therefore, targeting weaker mortar–stronger aggregate is the underlying principle of the proposed capacity-based mix design.

### 3.1 Failure Modes of Concrete Cubes Under Uniaxial Compression

In the absence of ITZ in high-strength concrete, which is a general expectation in the state-of-the art, two different modes of failure (if successfully designed) are hypothesized in this paper, namely, A: aggregate failure wherein mortar remains uncracked while aggregate initiates shear failure and M: mortar failure wherein mortar initiates cracking while aggregate remains intact. A mixed mode of failure ‘AM’ is also expected if not designed properly. Both the failure modes (A and M) with some expected behaviours are briefly discussed below.

#### 3.1.1 Failure Mode A: Aggregate Shear Failure

Let this failure mode of concrete (Fig. 6) be defined as  $c_{Afm} - \phi_{Afm}$  (cohesion and shear angle, respectively). Cohesion of concrete is lost due to shear failure of aggregate and let the experimental observations be, i)  $\sigma_{NC}^{Afm}$  = vertical strength/stress at failure and ii)  $\alpha^{Afm}$  ( $\pi/4 \leq \alpha^{Afm} \leq \pi/2$ ) = orientation of the failure plane. One may write:

$$\phi_{Afm} = 2\alpha^{Afm} - \frac{\pi}{2} \quad \left( \frac{\pi}{4} \leq \alpha^{Afm} \leq \frac{\pi}{2} \right), \quad (16)$$

$$\frac{\sigma_{CH}^{Afm}}{\sigma_{NC}^{Afm}} = \frac{1 - \sin \phi_{Afm}}{\cos^2 \phi_{Afm}}, \quad (17)$$

$$c_{Afm} = \frac{\sigma_{NC}^{Afm}}{2} \left( \frac{1 - \sin \phi_{Afm}}{\cos \phi_{Afm}} \right), \quad (18)$$



**Fig. 6** Aggregate failure mode (crack going through aggregates)—adapted from Zhang and Islam (2012)

$$\tau_{NC}^{Afm} = \sigma_{NC}^{Afm} \tan \phi_{Afm} + c_{Afm} = \frac{\sigma_{NC}^{Afm}}{2} \cos \phi_{Afm}. \quad (19)$$

Since the cohesion of concrete is lost due to shear failure of aggregate,  $c_{Afm} \approx c_{agg}$  and afterwards, mortar offers considerable resistance until the shear failure of concrete cube leading to  $\phi_{Afm} \gg \phi_{agg} \approx 0$ . In absence of ITZ, the aggregates may also be assumed as confined by the hardened mortar in concrete cubes. Since  $\phi_{agg} \approx 0$ , such confinement does not increase the shear strength (Fig. 4).

#### 3.1.2 Failure Mode M: Mortar Shear Failure

Let this failure mode of concrete be defined as  $c_{Mfm} - \phi_{Mfm}$  (Fig. 7). Cracks propagating through mortar is clearly evident from zoomed in view. Cohesion of concrete is lost due to shear failure of mortar and let the experimental observations be: i)  $\sigma_{NC}^{Mfm}$  = vertical strength / stress at failure and ii)  $\alpha^{Mfm}$  ( $\pi/4 \leq \alpha^{Mfm} \leq \pi/2$ ) = orientation of the failure plane. One may write:

$$\phi_{Mfm} = 2\alpha^{Mfm} - \frac{\pi}{2} \quad \left( \frac{\pi}{4} \leq \alpha^{Mfm} \leq \frac{\pi}{2} \right), \quad (20)$$

$$\frac{\sigma_{CH}^{Mfm}}{\sigma_{NC}^{Mfm}} = \frac{1 - \sin \phi_{Mfm}}{\cos^2 \phi_{Mfm}}, \quad (21)$$

$$c_{Mfm} = \frac{\sigma_{NC}^{Mfm}}{2} \left( \frac{1 - \sin \phi_{Mfm}}{\cos \phi_{Mfm}} \right), \quad (22)$$

$$\tau_{NC}^{Mfm} = \sigma_{NC}^{Mfm} \tan \phi_{Mfm} + c_{Mfm} = \frac{\sigma_{NC}^{Mfm}}{2} \cos \phi_{Mfm}. \quad (23)$$



**Fig. 7** Sample representation for mortar failure mode (cracks propagating through mortar)

Since the cohesion of concrete is lost due to shear failure of mortar,  $c_{Mfm} \approx c_{mor}$  and afterwards, aggregate offers considerable resistance in addition to the frictional resistance of mortar until the shear failure of concrete cube leading to  $\phi_{Mfm} > \phi_{mor}$ .

While enforcing and targeting the mortar failure mode, the loss of cohesion in concrete should be initiated owing to that of the mortar. In other words, cohesion of aggregate should not fall below a certain threshold,  $c_{agg|min}$  which must be higher than the cohesion of mortar,  $c_{mor}$ . Hence, the mortar should be designed conforming to the target compressive strength of concrete and aggregate selection should comply with the requirement  $c_{agg} > c_{agg|min} > c_{Mfm} \approx c_{mor}$ . Further, initiation of the loss of cohesion due to that of mortar does not itself guarantee the occurrence of mortar failure mode. In order to ensure the same, the necessary condition is that the shear strength of aggregate must not be less than that of mortar failure mode of concrete. In other words,

$$\tau_{agg} \left( = c_{agg} = \frac{\sigma_{NC}^{agg}}{2} \right) > \tau_{NC}^{Mfm} \left( = \frac{\sigma_{NC}^{Mfm}}{2} \cos \phi_{Mfm} \right) \Rightarrow \sigma_{NC}^{agg} > \sigma_{NC}^{Mfm} \cos \phi_{Mfm}. \tag{24}$$

Further details on this threshold are reported elsewhere (Sharma, 2024).

#### 4 Proposed Mix Design Procedure

Drawing on the hypothesis and principle presented in the supplement (Section S3), a general framework for the capacity-based approach is proposed here that primarily incorporates several pre- and post-processing steps within the traditional mix design process. The associated flowchart is also presented in Fig. 8.

1. Perform compressive strength of coarse aggregate per Section S2 and select the batch conforming to the threshold given by Eq. (24).
2. Compute the target mean strength using 50% of the recommended dispersion with the target characteristic strength and perform the standard mix design process to arrive at the quantities of ingredients.
3. Excluding the coarse aggregates (with some adjustment in the water content for maintaining fluidity of the mix) and using different combinations/proportions of SCMs, estimate the 3-sample mean compressive strength of standard (70.6 mm as per IS 4031-P6, 1988) mortar cubes. The combination/proportion leading to maximum mortar strength is selected as the optimum to proceed further.
4. Accept the mix design if the mean mortar strength with optimum replacement of SCMs is ~90% of the target mean compressive strength of concrete. The mortar phase strength is expected to increase further with the inclusion of coarse aggregate through effect of confinement over non-zero friction angle.

5. If the mean strength of mortar phase is far below the target mean strength of concrete, reduce the w/b ratio and repeat the whole process until the required mean strength is achieved. One should ideally work out a new optimum proportion of SCMs at this stage, which however, is expected to be a plateau (schematically) rather than a sharp peak. Therefore, for simplicity, one can work with the same optimum combination of SCMs if w/b ratio is slightly altered.

6. Add coarse aggregates to prepare the concrete mix once the desired strength of mortar phase is achieved. This may introduce additional voids which can be filled up by increasing the water content/paste content and/or filler content. Several trials must be performed by increasing the water content and altering the SCM proportion until the target strength is achieved. The percentage of SCMs in concrete should be chosen higher than that of mortar (known from step-3) and in that case, the resulting concrete strength is always expected to be higher than its mortar phase (Hypothesis 3/4).

7. Once the strength is achieved, change the water content according to the slump required and adjust the fluidity of concrete.

### 5 Experimental Programme

#### 5.1 Raw Materials

##### 5.1.1 Cement

OPC grade 53 conforming to IS 269:2015 is used throughout the study. The specific gravity and fineness of the cement are computed as 3.12 and 281 m<sup>2</sup>/kg, respectively. The chemical composition of cement is presented in Table 1.

**Table 1** Chemical composition of cement, silica fume and metakaolin

Binder	Percent by weight							
	CaO	SiO <sub>2</sub>	Al <sub>2</sub> O <sub>3</sub>	Fe <sub>2</sub> O <sub>3</sub>	Na <sub>2</sub> O	K <sub>2</sub> O	TiO <sub>2</sub>	MgO
Cement	61.76	21.46	4.30	4.04	1.52	0.61	0.38	5.30
Metakaolin	0.39	96.88	-	-	0.56	0.06	1.35	0.08
Silica fume	-	> 85	-	-	-	-	-	-

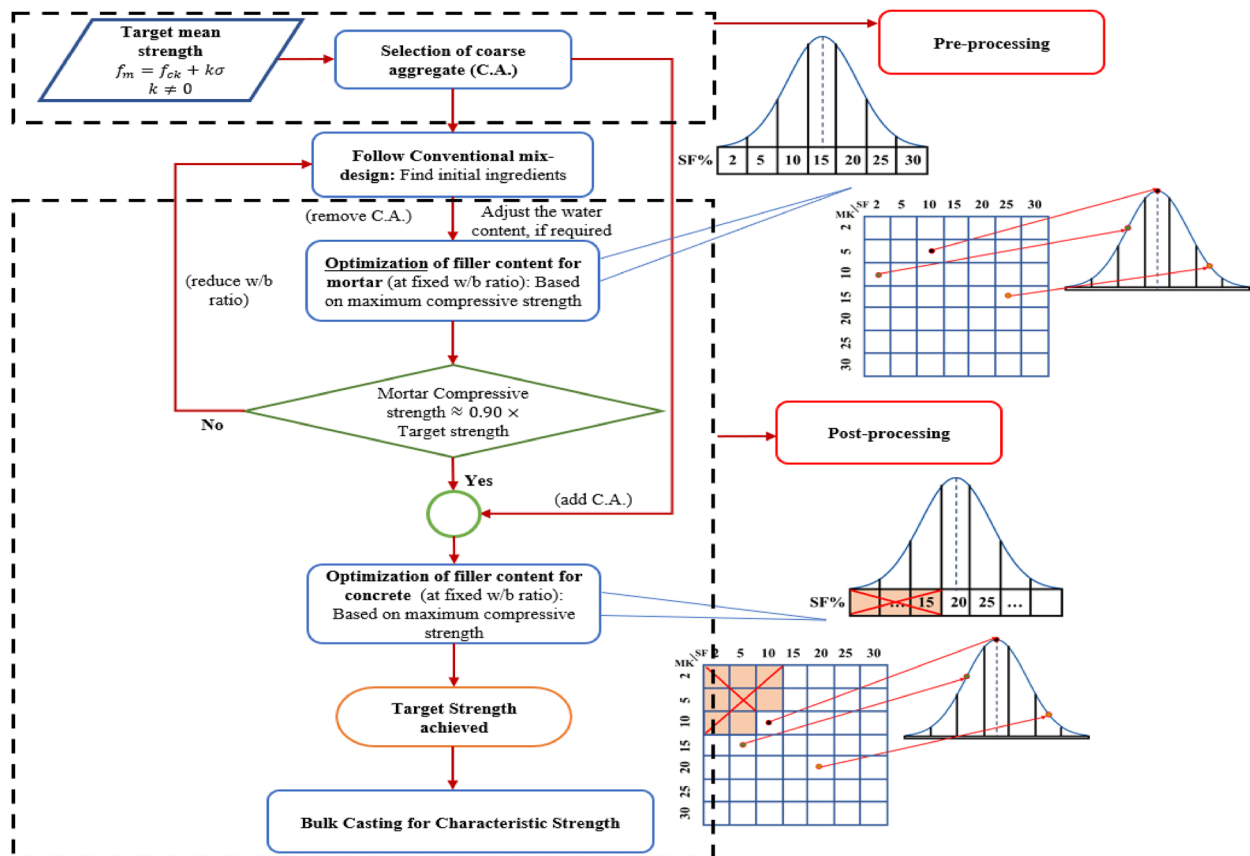


**Fig. 8** Flowchart for the capacity-based mix design framework

**Table 2** Manufacturer’s specifications for silica fume and metakaolin

	Specific gravity	Bulk density (kg/m <sup>3</sup> )	Average particle size (µm)
Silica fume	2.2	395	1.5–2.5
Metakaolin	2.5	300	1.5

**5.1.2 Supplementary Cementitious Materials (SCMs)**

SF and MK, procured from a local vendor, are used as SCMs through partial replacement of cement. Chemical composition and manufacturer specifications are presented in Tables 1 and 2, respectively. The particle size distribution is determined by the laser diffraction particle size analyser (Fig. 9). The D10, D50 and D90 of SF are found to be 1.09, 10.57, 27.05 microns, respectively. This larger particle size indicated in the distribution curve is due to the agglomeration of very fine particles. Since as-produced SF offers ample challenges while handling, it is generally supplied in the dry densified form. An efficient superplasticizer is required to disperse and deflocculate the agglomerated silica fume particles during mixing. The abrasive action of aggregates during mixing also helps in the deflocculation of SF particles. Similarly, D10, D50 and D90 of MK are 1.08, 21.93 and 48.92 microns, respectively. Observation of SEM images (Fig. 10) indicates that SF particles show a spherical morphology with smooth surface texture while MK displays an assemblage of hexagonal and irregular shapes.

**5.1.3 Fine Aggregate**

River sand conforming to the grading zone II of IS 383:2016 is used as fine aggregate. Figure 9 presents the particle size distribution of river sand used in this paper. The water absorption, specific gravity and fineness modulus of the river sand are determined through tests conforming to applicable IS codes and noted as 2.62, 0.51 and 2.76, respectively.

**5.1.4 Coarse Aggregate**

Crushed gravel with a nominal maximum size of 12.5 mm is procured from 4 different local vendors followed by sieving. The aggregates retained in 12.5 mm sieve are discarded from further consideration. The compression test is conducted as discussed in the supplement (Section S2) followed by the construction of average stress–strain plots for each of the four sample sets. The results are summarized in Fig. 11. Vendor 1 appears to be the best and is selected based on dual criteria: average compressive stress at the end of the test (50% normalized displacement per Section S2) and the associated dispersion. Higher average stress with lower dispersion

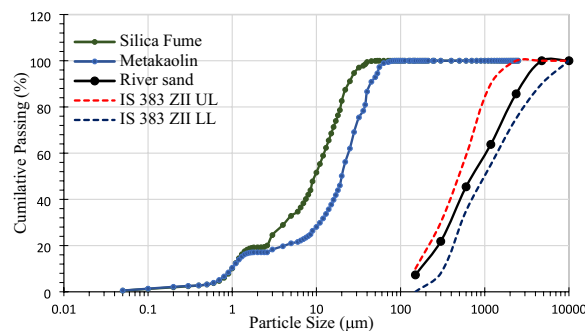


**Fig. 9** Particle size distribution of silica fume, metakaolin and sand

is an indicator of better quality. The average compressive strength of the aggregate from Vendor 1 is around 106 MPa.

M95 grade of concrete (characteristic strength ~ 95 MPa) is considered for the implementation of proposed capacity-based mix design. Indian Standard recommends a dispersion of 6 MPa for M80 (expected to increase for M95) and 50% of that is considered here as the proposed framework is aimed to deliver improved quality of concrete. The target mean strength is  $95 + 1.65 \times 3 \sim 100$  MPa and  $\sigma_{NC}^{Mfm} = 100$  MPa is considered in Eq. (24). However,  $\phi_{Mfm}$  required at this stage is not known and a lower bound  $\phi_{Mfm} \approx \phi_{mor}$  may suffice for the estimation of threshold aggregate strength. This lower bound may be considered as  $\phi_{Mfm} \approx \phi_{mor}$ .

Contingent on the mean target strength of 100 MPa, the w/b ratio of 0.28 is adopted and the mix design is carried out using standard procedure. Removing the coarse aggregates, 70.6 mm cubes are cast for mortar phase and the estimation of  $\phi_{mor}$ . Three mortar phase mixes of water content 202 kg/m<sup>3</sup>, 180 kg/m<sup>3</sup> and 160 kg/m<sup>3</sup> are prepared and three cubes from each mix are tested at 7 and 14 days age. Friction angles for mortar cubes are estimated in the range of 50 ~ 55 degrees at 7 days and 40 ~ 50 degrees at 14 days. Prima facie here is an estimate of  $\phi_{mor}$  at 28 days. Owing to this arguably decreasing trend towards the matured state (that might also be contributed from the development of cohesion and requires further study) and  $\phi_{mor}$  is assumed in an average sense as 40 degrees. The threshold compressive strength of aggregate is computed per Eq. (24) as ~ 77 MPa and clearly, the selected aggregate (~ 106 MPa) qualifies. The specific gravity and water absorption are further determined as per IS 2386:1963 part III and noted as 2.82 and 1.5%, respectively.

**5.1.5 Water and Superplasticizer**

Potable tap water available in the laboratory is used for mixing. Polycarboxylic-ether (PCE) based

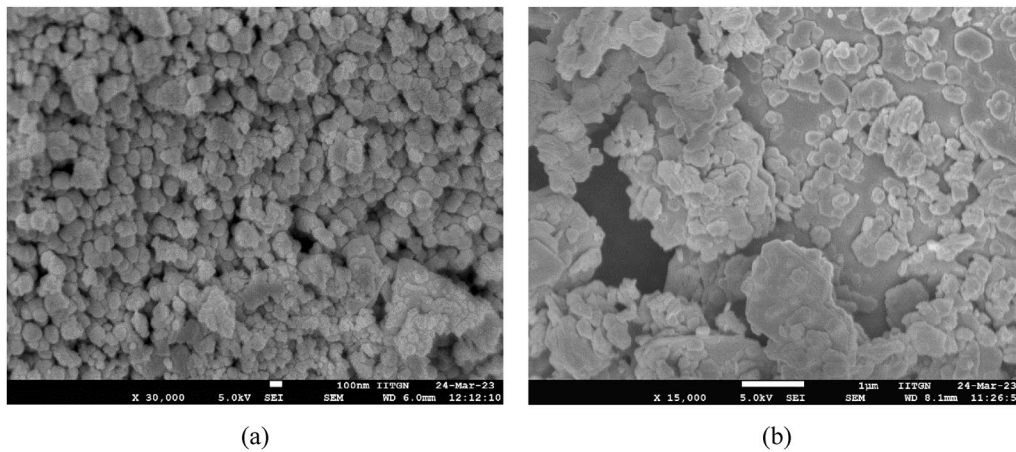
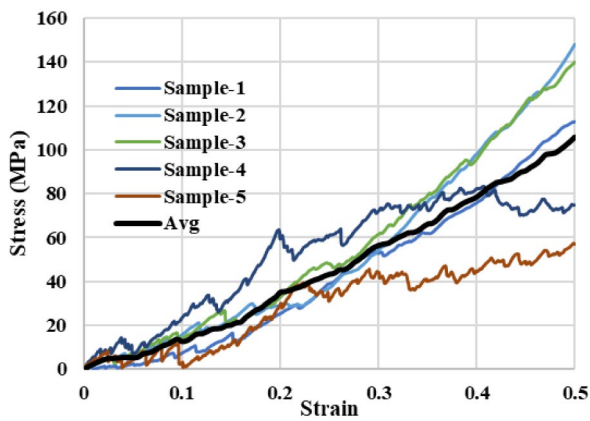
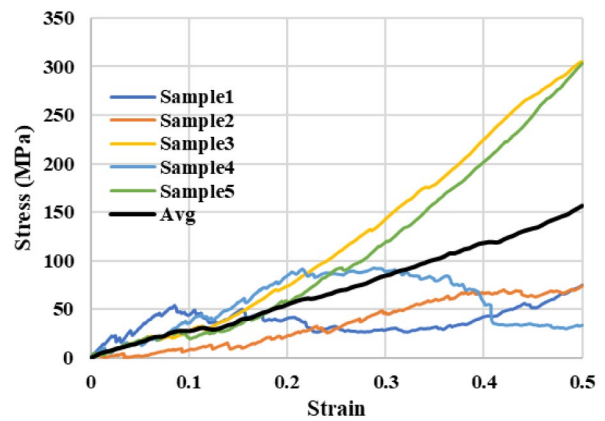


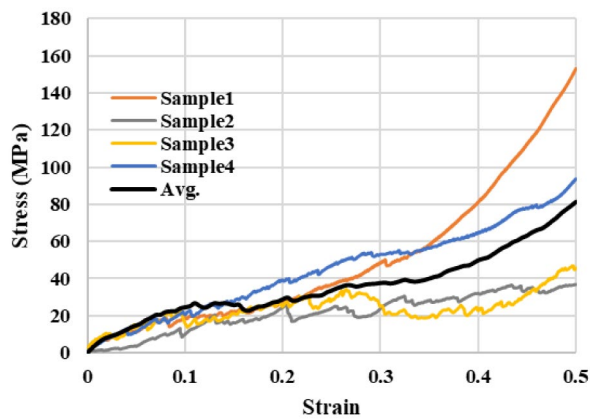
**Fig. 10** SEM images depicting morphological features of **a** silica fume, **b** metakaolin



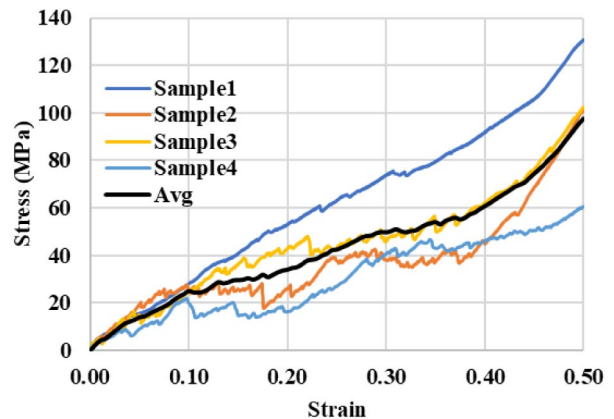
(a) Vendor-1



(b) Vendor-2



(c) Vendor-3



(d) Vendor-4

**Fig. 11** Stress–strain relationships for coarse aggregate for different vendors

superplasticizer (conforming to IS 9103:1999) manufactured by BASF with a solid content of 36% is used @1.31% (liquid dosage) by weight of binder content in all the mixes. The other details about the superplasticizer are available elsewhere (Mushtaq et al., 2022).

### 5.2 Mix Proportions

Associated with the target mean strength of 100 MPa for M95 concrete, w/b ratio of 0.28 is adopted and the mix design is carried out to arrive at the initial quantities. Varying combinations of SF and MK are used as a partial replacement of cement up to 15% (Table 3) and the optimum combination is worked out in the mortar phase by removing the coarse aggregate from the mix design. The w/b ratio is further reduced to 0.25 and 0.23 in the subsequent trials as the target mean strength of mortar phase (~0.9×100=90 MPa) was not achieved. Once the required strength in mortar phase is achieved with w/b ratio of 0.23, coarse aggregate is added back to design the concrete mix (using the same optimum combination of SF and MK as obtained in mortar phase). Two concrete mixes are designed; first without any change in the water content, i.e. 190 kg/m<sup>3</sup> and next by increasing the water content/paste content (208 kg/m<sup>3</sup>) to overcome the additional voids created due to coarse aggregate. Further, different combinations of SF and

MK, but subjected to two constraints, are used in concrete while targeting the mean compressive strength. Higher SF content than MK refers to the first constraint and the rationale of which is discussed later in this section. The second constraint is to adopt higher SF-MK content than the optimum replacement level at the mortar phase with the same w/b ratio of 0.23. This is an important step as discussed in hypothesis 4 (Section S3 in the supplement) to ensure higher concrete strength as compared to that of its mortar phase. Once the optimum combination of SF and MK in concrete at w/b ratio of 0.23 is determined, the same composition is selected as the final mix for bulk casting to assess the characteristic compressive strength and the associated dispersion. Additionally, the same combination of SF and MK is also studied at 0.25 w/b ratio for a comparative assessment of the underlying conservativeness involved in the proposed capacity-based mix design. The mix proportions for different concrete mixes used in this study are presented in Table 3, whereas the associated nomenclature is defined below.

#### 5.2.1 Designation of the Mixes

The concrete mixes are designated as C-SXMY-Q-R. Here ‘S’ and ‘M’ denote silica fume and metakaolin,

**Table 3** Mix proportions of concrete

Mix	SF (%)	MK (%)	w/c ratio	Mix proportions (kg/m <sup>3</sup> )						
				Cement	SF	MK	sand	Coarse aggregate	Water	Superplasticizer (solid)
w/b=0.28										
CC-0.28-165	0	0	0.28	590	0	0	657	1070	165	2.8
C-S5M5-0.28-165	5	5	0.28	530	30	30	644	1070	165	2.8
C-S7M5-0.28-165	7	5	0.28	519	41	30	641	1070	165	2.8
C-S10M5-0.28-165	10	5	0.28	501	59	30	637	1070	165	2.8
C-S5M7-0.28-165	5	7	0.28	519	30	41	641	1070	165	2.8
C-S5M10-0.28-165	5	10	0.28	501	30	59	637	1070	165	2.8
C-S7M7-0.28-165	7	7	0.28	508	41	41	639	1070	165	2.8
w/b=0.25										
C-S7M7-0.25-190	7	7	0.25	654	53	53	425	1070	190	3.61
C-S7M7-0.25-208	7	7	0.25	714	58	58	596	784	208	3.94
C-S10M7.5-0.25-205	10	7.5	0.25	676	82	62	600	790	205	3.90
w/b=0.23										
C-S7M7-0.23-210	7	7	0.23	782	64	64	557	745	210	4.32
C-S10M8.5-0.23-210	10	8.5	0.23	742	91	71	553	739	210	4.32
C-S10M7.5-0.23-210	10	7.5	0.23	751	91	68	554	740	210	4.32
C-S8.5M7.5-0.23-210	8.5	7.5	0.23	765	77	68	555	742	210	4.32
C-S8.5M8.5-0.23-210	8.5	8.5	0.23	756	77	77	554	741	210	4.32
C-S7.5M7.5-0.23-210	7.5	7.5	0.23	774	68	68	556	743	210	4.32

respectively, with ‘X’ and ‘Y’ as their respective replacement levels in percentage. ‘Q’ and ‘R’ indicate the w/b ratio and water content, respectively, used in the mix. For example, C-S7M5-0.28-165 indicates a concrete mix consisting of 7 and 5% replacement levels for SF and MK, respectively. The w/b ratio for the mix is 0.28, whereas the water content is 165 kg/m<sup>3</sup>. The same nomenclature is also used for mortar but with ‘C’ replaced by ‘M’.

**5.2.2 Rationale Behind Using Higher SF Content than MK**

There have been conflicting inferences on the effectiveness of using SF-MK as ternary blends to increase the strength of concrete. Nevertheless, SF is more commonly used as an SCM in HSC and expected to react faster during the early stages due to its ultra-fine particles and high pozzolanic activity. A larger amount of SF when compared with MK is also required to weaken the significance of the "wall effect" and thereby improving the ITZ. It is also observed during the preliminary trials that the mixes with higher SF content exhibit greater strength than those with higher MK content. Hence, in all subsequent trials SF content is kept higher than that of MK.

**5.3 Testing Procedure**

Testing programme consists of (i) compressive strength of coarse aggregate (Section S2 in the supplement) to assess its suitability for use in M 95 concrete and (ii) compressive strength of concrete and mortar phase. Compression testing machine (CTM) of 3000 kN capacity at a strain rate of 1 mm/mm is used for this assessment. A total of 9 cubes of concrete as well as its mortar phase are cast for each mix and tested at 7, 14 and 28 days. Details on mixing, casting and curing are presented in the supplement (Section S4). At the completion of the curing age, the specimens are taken out of the curing tank, allowed to air dry for about an hour and placed within the CTM for testing. The average of 3 specimens is reported as the achieved mean strength of the mix.

**6 Results and Discussion**

**6.1 Achieving Strength and Finding the Optimum Combination in the Mortar Phase**

Fig. 12 shows significant improvement in average mortar compressive strength (at w/b ratio of 0.28) for all the mixes containing SF and MK as compared to the mortar phase of control concrete (CC-0.28-165) at 14 days. However, only the mixes M-S5M7-0.28-165 and M-S7M7-0.28-165 show around 6% and 14%, respectively, increase whereas the strength of other mixes remains nearly the same when compared with the control concrete at 28 days. The maximum 3-sample average strength is observed in the mix M-S7M7-0.28-165 (~83 MPa). The maximum individual strength of 92 MPa is also observed

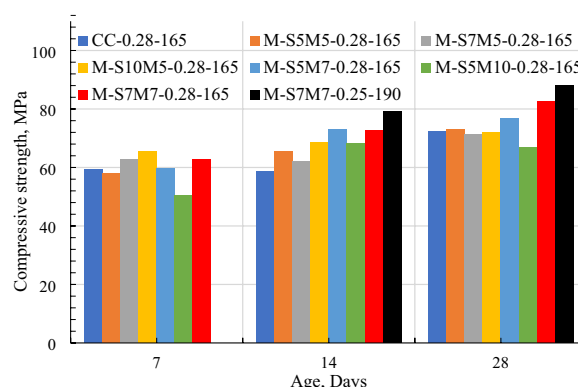


**Fig. 12** Compressive strength results for mortar phase with different combinations of SF and MK

in this mix. The same mix is further explored at lower w/b ratio of 0.25 with a modified water content of 190 kg/m<sup>3</sup> to improve the mean strength (Fig. 12). A 3-sample average strength of around 88 MPa is achieved, which is again slightly lower than the required 90 MPa. Apparently, another trial is required with somewhat lower w/b ratio, say 0.23 followed by an assessment of the strength in mortar phase. However, the desired mortar strength is assumed to be achieved with w/b ratio of 0.23 (owing to the small difference) and the mix design is proceeded to the next step (without further assessment of the mortar) for the assessment of compressive strength of concrete. Nevertheless, the compressive strength results with 0.23 w/b ratio are shown in Sect. 7 for both mortar phase and concrete.

**6.2 Compressive Strength in Concrete**

The mix C-S7M7-0.25-190, representing the concrete prepared by adding the coarse aggregate to its mortar phase (Sect. 5.1) without any adjustment in the paste/water content, shows a significant reduction in the compressive strength: 15% and 13% reduction at 14 days and 28 days, respectively. Here, the comparison is carried out between the results of M-S7M7-0.25-190 and C-S7M7-0.25-190 at 14 days and 28 days. This reduction in the compressive strength is attributed to the probable increase in voids content or disturbances in the packing of already optimized mortar phase due to the inclusion of coarse aggregates. Once the water content is increased to 208 kg/m<sup>3</sup>, the compressive strength in concrete approaches to its mortar phase strength (~88 MPa at 28 days). Hence, inclusion of coarse aggregates in mortar demands an increase in the paste content to fill the possible additional voids. The compressive strength of resulting concrete should approach that of the mortar or even surpass it in absence of ITZ (Fig. 13). Finally, the resulting compressive strength from the mix C-S7M7-0.23-210

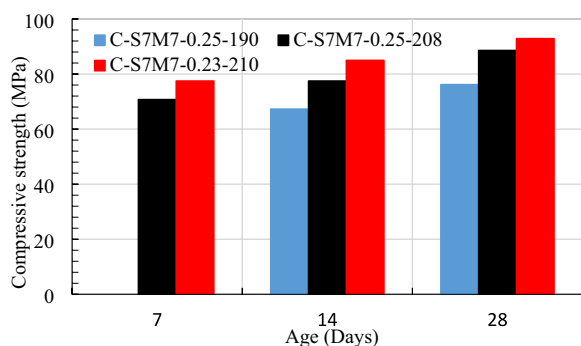


**Fig. 13** Compressive strength results for concrete with 7% SF and 7% MK (comment: the compressive strength test for M-S7M7-0.25-190 and C-S7M7-0.25-190 at 7 days were not conducted)

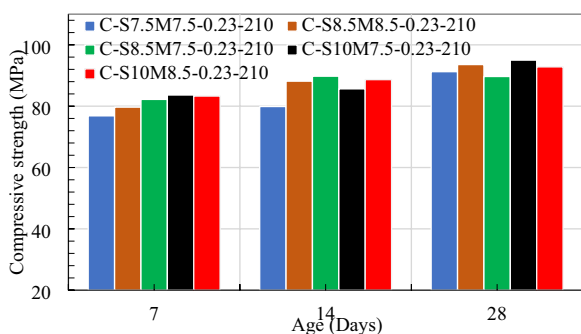


**Fig. 14** Compressive strength results of concrete with different combinations of SF and MK

(SF-MK content is not changed at this stage) are noted as 77.5, 85 and 92.9 MPa at 7, 14 and 28 days, respectively. The average 28-day strength achieved is very close but somewhat less than the target mean strength of 100 MPa. This will be achieved by improving only the SF-MK content (at the same w/b ratio of 0.23).

**6.3 Optimizing the SF and MK Combination in Concrete**

Several replacement levels of SF-MK above S7M7 at w/b ratio of 0.23 with water content of 210 kg/m<sup>3</sup> are tried and the 3-sample average strengths are compared in Fig. 14. The mix C-S10M7.5-0.23-210 leads to a maximum 3-sample average concrete strength of 95 MPa. The same mix also shows the least variation in concrete strength when compared with all other mixes. It is also interesting to note that 3-sample average strength does not fall below 90 MPa regardless of the replacement level of SF and MK. Fig. 15 compares 3-sample average mortar phase strength against the resulting compressive strength of concrete. When the replacement level of SF and MK is near the optimum level of mortar phase (S7M7), the resulting 28-day concrete strength is close

to that of the mortar phase (Fig. 15a). As the replacement level is increased up to 10% SF and 7.5% MK, the strength of concrete increases nominally but that of mortar phase reduces substantially (Fig. 15b–d), which is intended. Further increase in the replacement level apparently reduces the concrete strength at 28 days. As the maximum strength (though slightly lower than the target mean strength, 95 MPa against 100 MPa) along with the least variation is obtained in the mix C-S10M7.5-0.23-210, this composition is selected as the final mix for bulk casting to study the dispersion and the characteristic compressive strength. In addition, the bulk casting are also carried out for this replacement level at w/b ratio of 0.25 for assessing the dispersion and underlying conservativeness.

**6.4 Bulk Casting**

Statistical inferences are generally asymptotically unbiased. Aleatory variables are generally assumed to be normally distributed. Parameter estimation such as estimation of statistical expectation (mean) and variance (square of dispersion) from the observed realization requires sufficiently large sample space, if not infinite. Typically, a minimum of 30 specimens should be cast to estimate the dispersion/standard deviation and hence, the characteristic strength of concrete. The available concrete mixer enables the casting of maximum 10 cube specimens in one batch. Hence, the construction of a sample space of 30 specimens is likely to introduce the batch-to-batch variability in the estimation of parameters. Nevertheless, only 20 samples are used in this paper for estimating the bulk characteristics. The bulk casting is carried out in two batches, namely BC1 and BC2. Each batch consists of 10 cube specimens.

The 28-day compressive strength results are presented in Fig. 16 and also in Table 4. Fig. 16a–c presents the results for w/b ratio 0.23. Batch-1 leads to the characteristic strength of 96.3 MPa with a standard deviation and coefficient of variation as 2.8 MPa and 2.8%, respectively (Fig. 16a). Batch-2 results in a characteristic strength of 95.11 MPa with a standard deviation of 1.86 MPa and coefficient of variation as 1.9% (Fig. 16b). Clearly, the individual batches do not exhibit the expected normal distribution owing to the inadequate sample size (10 specimens). Fig. 16c presents the histogram for the combined 20 samples from two batches that relatively better resembles to the normal distribution. The resulting characteristic strength is noted as ~95 MPa with standard deviation and coefficient of variation as 2.74 MPa and 2.75%, respectively. Clearly, the target M95 concrete is achieved with overall coefficient of variation as 2.75% which falls in the class of excellent quality control as per the control standards given in ACI 214R-11: The class of

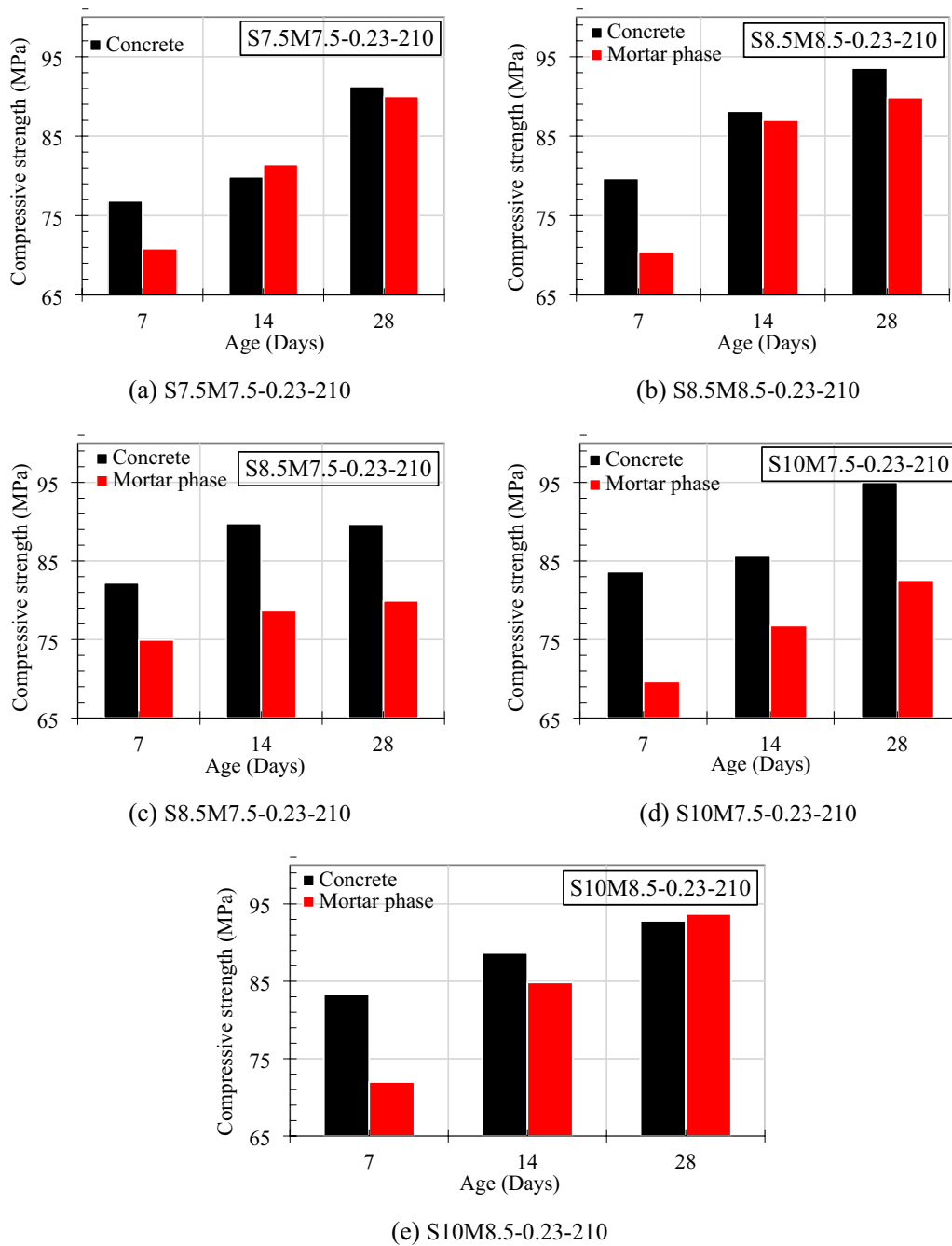
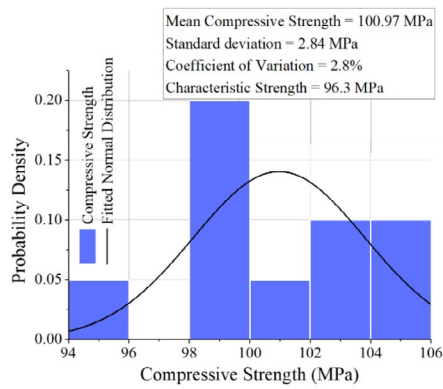


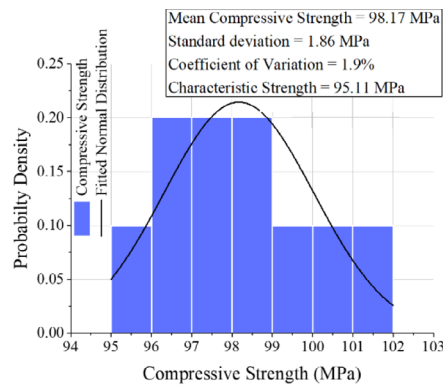
**Fig. 15** Comparison of compressive strength results of concrete and the corresponding mortar phase

operation is classified as excellent if the coefficient of variation is below 3.5% for concrete with cylinder characteristic strength greater than 35 MPa (~cube characteristic strength exceeding 44 MPa). The resulting standard deviation is expected to be further reduced if larger mixer is used enabling all 20 specimens from the same batch and thereby eliminating the batch-to-batch variability.

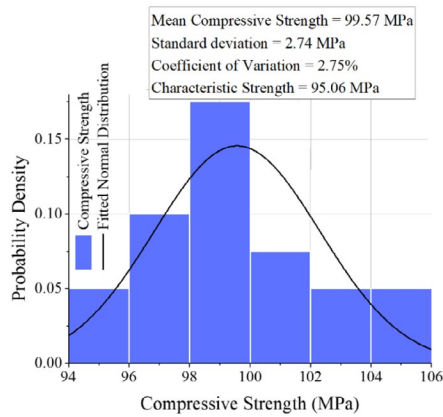
Similar results are presented in Fig. 16d-f for the w/b ratio of 0.25. The resulting characteristic strength is 90.6 MPa with a standard deviation and coefficient of variation as 3 MPa and 3.15% (<3.5), respectively (BC). It must be noted that C-S10M7.5-0.25-205 mix does not represent the appropriate finer content (but close to it!) for w/b ratio of 0.25 conforming to the proposed capacity-based framework. These results



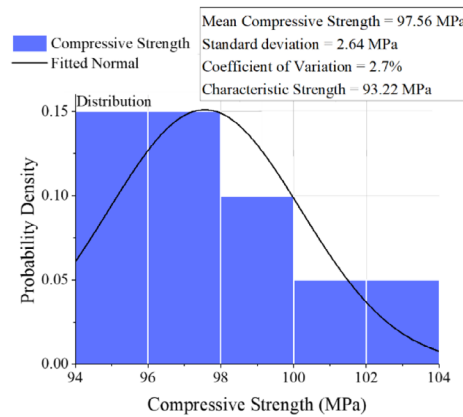
(a) Bulk casting BC1 (10 specimens)-w/b = 0.23



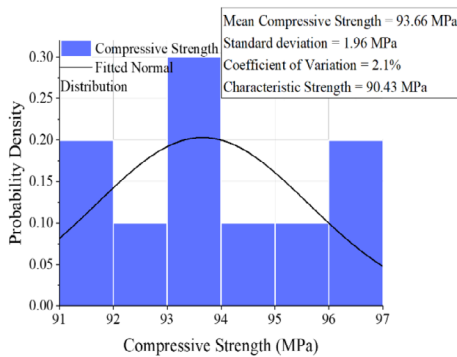
(b) Bulk casting BC2 (10 specimens)-w/b = 0.23



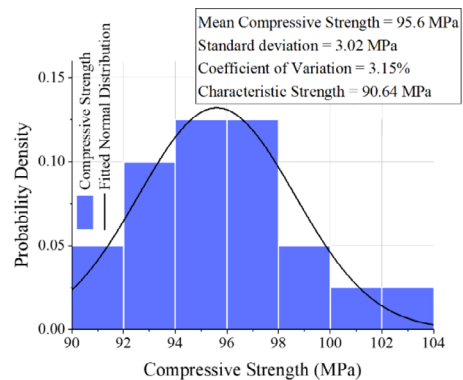
(c) Bulk casting combined BC1 and BC2 (20 specimens)-w/b = 0.23



(d) Bulk casting BC1 (10 specimens)-w/b = 0.25



(e) Bulk casting BC1 (10 specimens)-w/b = 0.25



(f) Bulk casting combined BC1 and BC2 (20 specimens)-w/b = 0.25

**Fig. 16** Compressive strength distribution for bulk casting

are included here to demonstrate the underlying conservatism involved in the mix design of M95 concrete using the proposed framework. Further, the resulting

low dispersion again supports the claim of excellent quality control in the proposed capacity-based mix design.

**Table 4** Compressive strength results for bulk casting at 28 days

w/b	0.23		0.25	
	BC 1	BC 2	BC 1	BC 2
28-day compressive strength (MPa)	101.1	101.1	98.6	96.07
	95.5	98.8	98.2	93.3
	99.8	97.2	94.5	93.1
	102.8	97	102.7	91.2
	104.7	96.6	96.2	93
	99.7	98.8	97.9	96.8
	104.9	100.3	95.1	92
	99.4	96.1	96.8	91.4
	99.4	95.9	94.9	94
	102.4	99.9	100.7	95.7
Mean (MPa)	100.97	98.17	97.56	93.66
St. Dev. (MPa)	2.84	1.86	2.64	1.96
$f_{ck}$ (MPa)	96.3	95.11	93.22	90.43
COV (%)	2.8	1.9	2.7	2.1
Overall mean (MPa)	99.57		95.6	
Overall St. Dev. (MPa)	2.74		3.02	
Overall COV (%)	2.75		3.15	
Overall $f_{ck}$ (MPa)	95.06		90.64	

**7 Mix Design by IS 10262:2019**

While performing mix design for M95 concrete conforming to IS 10262:2019, the recommended w/b ratio may be worked out as 0.25. The SF-MK replacement considered here is same as that resulted from the proposed capacity-based mix design, i.e. S10M7.5. Resulting mix proportions are shown in Table 5. Three batches of 10 samples are cast and the resulting 28-day compressive strengths are shown in Table 6. The coefficient of variation is found to be less than 3.5% (2.5%) as earlier, with a characteristic strength of 90.9 MPa. The strength of mortar phase is also determined and interestingly found to be less than that of concrete, as expected. The average 28-day compressive strength of the mortar phase is observed to be 77 MPa (details are not shown here for the brevity).

This apparent resemblance of mix design recommended by IS 10262:2019 to the proposed capacity-based framework (Table 4, w/b=0.25) is primarily attributed to the following: (i) coarse aggregates are selected after determining their suitability as per Eq. 24; (ii) SCM

content used is borrowed from the capacity-based mix design process; and (iii) the paste content is also borrowed from the capacity-based mix design. However, one may expect substantial dispersion in compressive strength if uncontrolled aggregate and/or any other combination of SF-MK, especially that less than S7M7 is used in the mix.

**8 Conclusions**

The current mix design frameworks often lack a proper control over the potential failure modes of concrete despite recommendations on the quality control of the raw materials. This paper identifies the possible failure modes in concrete and thereby proposes a capacity-based methodology to eliminate all the undesirable modes of failure for example, suppressing (postponing) the aggregate failure mode and preponing the mortar failure mode. Dispersion of the aggregate phase strength is relatively higher (than that of the mortar phase) due to (i) various uncertainties contributed from the natural sources and (ii) the limited scope of reducing the epistemic uncertainty during mix design (as it is used without any processing). However, the mortar strength can be controlled by carefully designing the relative proportion of the constituents, which significantly reduces the associated epistemic uncertainty. Therefore, targeting weaker mortar–stronger aggregate is the underlying principle of the proposed capacity-based mix design. In other words, if concrete can be engineered to fail predominantly through the mortar mode, it will result in a superior quality control and minimal variation. This paper also revisits the mix design method recommended in IS 10262:2019 through the window of proposed capacity-based approach. The concrete mix (grade M95) designed with the proposed capacity-based approach shows an overall coefficient of variation below 3.5% indicating excellent quality control. The key conclusions that can be drawn from the limited investigation carried out in this paper are given below:

1. Assuming Mohr–Coulomb theory, the cohesion and friction angle of concrete or mortar cubes can be obtained using one single uniaxial unconfined compression test. Such a framework is proposed in this paper. This approach minimizes the errors contributed from sample-to-sample variation. Orientation

**Table 5** Mix proportions as per IS 10262:2019

Mix	SF (%)	MK (%)	w/c ratio	Mix proportions (Kg/m <sup>3</sup> )						
				Cement	SF	MK	Sand	Coarse aggregate	Water	Superplasticizer (solid)
C-S10M7.5–0.25–200	10	7.5	0.25	660	80	60	603.18	785.76	200	3.8

**Table 6** Compressive strength results of bulk casting of concrete at w/b 0.25 as per Indian Standard

w/b	0.25		
	BC 1	BC 2	BC 3
28-day compressive strength (MPa)	93.08	92.44	93.86
	93.19	95.45	96.32
	95.94	95.42	97.71
	93.24	95.99	96.53
	92.37	94.15	98.27
	99.19	97.58	97.19
	92.01	96.19	99.5
	94	91.49	94.41
	94.51	93	99.67
	91.72	91.24	97.01
Mean (MPa)	93.93	94.30	97.05
St. Dev. (MPa)	2.23	2.17	1.91
$f_{ck}$ (MPa)	90.24	90.72	93.9
COV (%)	2.38	2.30	1.97
Overall mean (MPa)	94.92		
Overall St. Dev. (MPa)	2.42		
Overall COV (%)	2.55		
Overall $f_{ck}$ (MPa)	90.94		

of the failure plane of fractured specimen provides the necessary supplementary information.

- The coarse aggregate must meet a certain strength (threshold) to ensure a controlled mortar failure and to prevent the uncontrolled aggregate failure in concrete leading to significant reduction in dispersion. This is in line with what is required in the seismic design of structures.
- Inclusion of coarse aggregate after optimizing the mortar phase is likely to disturb the packing leading to the creation of extra voids and thereby decreasing the strength. Hence, when adding the coarse aggregate following the proposed capacity-based mix design framework, the paste content should be increased and the SCM content should be re-optimized. Resulting concrete strength in such cases may approach or even surpass the mortar phase strength.
- Keeping the strength of the mortar phase lower than that of the concrete ensures that the concrete will always fail in the mortar failure mode leading to an excellent quality of concrete with reduced standard deviation. The sample illustration on 95 MPa concrete shows ~3 MPa standard deviation (~3% coefficient of variation).
- Similar dispersion can also be achieved if it is possible to arrive at the similar composition as that of capacity-based mix design while designing the concrete mix following IS 10262:2019. Since the opti-

mal SCM content in mortar is not known a priori, unlike the capacity-based framework, a wide range of combinations are required to be explored. Computation of dispersion associated with each combination also requires a sample size of 20 (specimens). Consequently, this process can be costly, laborious and time-consuming, although possible.

- Uncertainty in the prediction of concrete strength can alter the sequence of plastic hinge formation during a seismic event, potentially leading to the undesirable mode of brittle shear failure. If the characteristic compressive strength of concrete is underestimated, the moment capacity of columns will be significantly reduced as compared to the plastic capacity of beams (which is primarily governed by the yield stress of the rebar and the associated overstrength, i.e. the ratio of ultimate to yield strength). This is likely to attract non-compliance of otherwise assumed strong column–weak beam principle.

Overall, variation in concrete strength owing to the uncertainty in adopted mix design framework may have a considerable impact on the seismic design which can be addressed through stringent quality control and the proposed capacity-based mix design framework offers a viable choice.

**Abbreviations**

A	Aggregate failure wherein mortar remains uncracked while aggregate initiates shear failure
M	Mortar failure wherein mortar initiates cracking while aggregate remains intact
AM	Mixed mode of failure
CTM	Compression testing machine
CC	Control concrete
GGBS	Ground granulated blast furnace slag
HPC	High-performance concrete
HSC	High-strength concrete
IS	Indian Standard
ITZ	Interfacial transition zone
LWA	Low weight aggregate
MK	Metakaolin
NSC	Normal strength concrete
OPC	Ordinary Portland cement
PCE	Polycarboxylic-ether
SCMs	Supplementary cementitious materials
SEM	Scanning electron microscopy
SF	Silica fume
D10	The diameter at which 10% of the particles in the sample are smaller.
D50	The diameter at which 50% of the particles are smaller and 50% are larger.
D90	The diameter at which 90% of the particles in the sample are smaller
w/b	Water/binder ratio
w/c	Water/cement ratio
c	Cohesion
$c_{agg}$	Cohesion of aggregate
$c_{mor}$	Cohesion of mortar
$c_{Afm}$	Cohesion governed by aggregate failure mode
$c_{Mfm}$	Cohesion governed by mortar failure mode
$c_{agg min}$	Minimum threshold value for cohesion of mortar

$\phi$	Angle of internal friction/ friction angle
$\phi_{agg}$	Friction angle of aggregate
$\phi_{mor}$	Friction angle of mortar
$\phi_{Afm}$	Friction angle governed by aggregate failure mode
$\phi_{Mfm}$	Friction angle governed by mortar failure mode
$\alpha$	Orientation of the failure plane
$\alpha_{WC}$	Orientation of the failure plane in presence of confining pressure
$\alpha_{NC}$	Orientation of the failure plane in without confining pressure
$\alpha^{Afm}$	Orientation of the failure plane governed by aggregate failure mode
$\alpha^{Mfm}$	Orientation of the failure plane governed by mortar failure mode
$P_{NC}$	Confining pressure
$\sigma_{WC}$	Confined compressive strength
$\sigma_{NC}$	Unconfined compressive strength
$\sigma_{NC}^{agg}$	Unconfined compressive strength of aggregate
$\sigma_{NC}^{Afm}$	Unconfined compressive strength governed by aggregate failure mode
$\sigma_{NC}^{Mfm}$	Unconfined compressive strength governed by mortar failure mode
$\sigma_{CH}$	Applied vertical stress at which cohesion is lost on the failure plane
$\sigma_{CH}^{Afm}$	Applied vertical stress at which cohesion is lost on the failure plane governed by aggregate failure mode
$\sigma_{CH}^{Mfm}$	Applied vertical stress at which cohesion is lost on the failure plane governed by mortar failure mode
$\sigma_{fp}^{WC}$	Normal stress at the failure plane with confinement
$\sigma_{fp}^{NC}$	Normal stress at the failure plane without confinement
$\sigma_{fp,CH}^{NC}$	Associated normal stress on the failure plane at which cohesion is lost without confinement
$\tau_{fp}^{WC}$	Shear stress at the failure plane with confinement
$\tau_{fp}^{NC}$	Shear stress at the failure plane without confinement
$\tau_{fp,CH}^{NC}$	Associated shear stress on the failure plane at which cohesion is lost without confinement
$\tau_{NC}^{Afm}$	Shear stress at the failure plane without confinement governed by aggregate failure mode
$\tau_{NC}^{Mfm}$	Shear stress at the failure plane without confinement governed by mortar failure mode
$\tau_{agg}$	Shear strength of aggregate

## Supplementary Information

The online version contains supplementary material available at <https://doi.org/10.1186/s40069-024-00722-8>.

Supplementary Material 1.

## Acknowledgements

This research is funded by Gujarat Council of Science and Technology, Department of Science and Technology, Government of Gujarat, India, under the Grant No. GUJCOST/ 2020-21/874. The authors also acknowledge Sika Viscocrete SKY for supplying the superplasticizer.

## Author contributions

DB—proposed the idea, performed conceptual design, interpreted the results, prepared the final draft, and managed the overall research; SM—performed the experiments, processed the data, generated and interpreted the results, and prepared the first draft; SS—performed the experiments, processed the data, generated and interpreted the results; ST—performed the experiments, processed the data, generated and interpreted the results.

## Funding

Gujarat Council of Science and Technology, Department of Science and Technology, Government of Gujarat, GUJCOST/ 2020-21/874, Dhiman Basu.

## Availability of data and materials

The datasets used and/or analysed during the current study are available from the corresponding author on reasonable request.

## Declarations

### Ethics approval and consent to participate

Not applicable.

### Consent for publication

Not applicable.

### Competing interests

The authors declare that they have no competing interests in this section.

Received: 3 February 2024 Accepted: 7 August 2024

Published online: 11 November 2024

## References

- Ahmad, M. R., & Chen, B. (2019). Experimental research on the performance of lightweight concrete containing foam and expanded clay aggregate. *Composites Part B Engineering*, 171, 46–60. <https://doi.org/10.1016/j.compositesb.2019.04.025>
- Bilal, H., Chen, T., Ren, M., Gao, X., & Su, A. (2021). Influence of silica fume, metakaolin and SBR latex on strength and durability performance of pervious concrete. *Construction and Building Materials*. <https://doi.org/10.1016/j.conbuildmat.2020.122124>
- Bogas, J. A., & Gomes, A. (2013). Compressive behavior and failure modes of structural lightweight aggregate concrete—Characterization and strength prediction. *Materials and Design*, 46, 832–841. <https://doi.org/10.1016/j.matdes.2012.11.004>
- Chen, J. J., Ng, P. L., Chu, S. H., Guan, G. X., & Kwan, A. K. H. (2020). Ternary blending with metakaolin and silica fume to improve packing density and performance of binder paste. *Construction and Building Materials*. <https://doi.org/10.1016/j.conbuildmat.2020.119031>
- Chu, S. H., Chen, J. J., Li, L. G., Ng, P. L., & Kwan, A. K. H. (2021). Roles of packing density and slurry film thickness in synergistic effects of metakaolin and silica fume. *Powder Technology*, 387, 575–583. <https://doi.org/10.1016/j.powtec.2021.04.029>
- Chu, S. H., & Kwan, A. K. H. (2019). Co-addition of metakaolin and silica fume in mortar: Effects and advantages. *Construction and Building Materials*, 197, 716–724. <https://doi.org/10.1016/j.conbuildmat.2018.11.244>
- Dushimimana, A., Niyonsenga, A. A., & Nzamurambaho, F. (2021). A review on strength development of high-performance concrete. *Construction and Building Materials*. <https://doi.org/10.1016/j.conbuildmat.2021.124865>
- Güneyisi, E., Gesoğlu, M., Karaoğlu, S., & Mermerdaş, K. (2012). Strength, permeability and shrinkage cracking of silica fume and metakaolin concretes. *Construction and Building Materials*, 34, 120–130. <https://doi.org/10.1016/j.conbuildmat.2012.02.017>
- Güneyisi, E., Gesoğlu, M., & Özbay, E. (2010). Strength and drying shrinkage properties of self-compacting concretes incorporating multi-system blended mineral admixtures. *Construction and Building Materials*, 24(10), 1878–1887. <https://doi.org/10.1016/j.conbuildmat.2010.04.015>
- Huynh, T. P., Ho, L. S., & Van Ho, Q. V. (2022). Experimental investigation on the performance of concrete incorporating fine dune sand and ground granulated blast-furnace slag. *Construction and Building Materials*. <https://doi.org/10.1016/j.conbuildmat.2022.128512>
- IS 10262. (2019). Concrete Mix proportioning – Guidelines (second revision). Bureau of Indian Standards.
- IS 4031-P6. (1988). Methods of Physical tests for hydraulic cement, Part 6: Determination of compressive strength of hydraulic cement (other than masonry cement), Bureau of Indian Standards.
- Jiang, C., Yang, Y., Wang, Y., Zhou, Y., & Ma, C. (2014). Autogenous shrinkage of high-performance concrete containing mineral admixtures under different curing temperatures. *Construction and Building Materials*, 61, 260–269. <https://doi.org/10.1016/j.conbuildmat.2014.03.023>
- Jóźwiak-Niedźwiedzka, D. (2005). Scaling resistance of high-performance concretes containing a small portion of pre-wetted lightweight fine aggregate. *Cement and Concrete Composites*, 27(6), 709–715. <https://doi.org/10.1016/j.cemconcomp.2004.11.001>

- Kayali, O. (2008). Fly ash lightweight aggregates in high performance concrete. *Construction and Building Materials*, 22(12), 2393–2399. <https://doi.org/10.1016/j.conbuildmat.2007.09.001>
- Lämmlein, T. D., Messina, F., Wyrzykowski, M., Terrasi, G. P., & Lura, P. (2019). Low clinker high performance concretes and their potential in CFRP-prestressed structural elements. *Cement and Concrete Composites*, 100, 130–138. <https://doi.org/10.1016/j.cemconcomp.2019.02.014>
- Ma, X., Liu, J., & Shi, C. (2019). A review on the use of LWA as an internal curing agent of high-performance cement-based materials. *Construction and Building Materials*, 218, 385–393. <https://doi.org/10.1016/j.conbuildmat.2019.05.126>
- Mo, Z., Han, Y., Jiang, L., Wang, J., & Gao, X. (2022). Strength properties and hydration of ultra-high-performance concrete incorporating calcined clay and limestone with steam curing regimes. *Case Studies in Construction Materials*. <https://doi.org/10.1016/j.cscm.2022.e01658>
- Mushtaq, S. M., Rajput, T., & Basu, D. (2022). Cement–superplasticizer compatibility and flow properties of binder paste and mortar using marsh cone and flow table method. *Indian Concrete Journal*, 96(9), 20–33.
- Nepomuceno, M. C. S., Pereira-de-Oliveira, L. A., & Pereira, S. F. (2018). Mix design of structural lightweight self-compacting concrete incorporating coarse lightweight expanded clay aggregates. *Construction and Building Materials*, 166, 373–385. <https://doi.org/10.1016/j.conbuildmat.2018.01.161>
- Piro, N. S., Mohammed, A. S., & Hamad, S. M. (2022). The impact of GGBS and ferrous on the flow of electrical current and compressive strength of concrete. *Construction and Building Materials*. <https://doi.org/10.1016/j.conbuildmat.2022.128639>
- Poon, C. S., Kou, S. C., & Lam, L. (2006). Compressive strength, chloride diffusivity and pore structure of high performance metakaolin and silica fume concrete. *Construction and Building Materials*, 20(10), 858–865. <https://doi.org/10.1016/j.conbuildmat.2005.07.001>
- Rossetti, A., Ikumi, T., Segura, I., & Irassar, E. F. (2021). Sulfate performance of blended cements (limestone and illite calcined clay) exposed to aggressive environment after casting. *Cement and Concrete Research*. <https://doi.org/10.1016/j.cemconres.2021.106495>
- Safuddin, M., West, J. S., & Soudki, K. A. (2010). Hardened properties of self-consolidating high performance concrete including rice husk ash. *Cement and Concrete Composites*, 32(9), 708–717. <https://doi.org/10.1016/j.cemconcomp.2010.07.006>
- Shah, V., & Scott, A. (2021). Hydration and microstructural characteristics of MgO in the presence of metakaolin and silica fume. *Cement and Concrete Composites*. <https://doi.org/10.1016/j.cemconcomp.2021.104068>
- Sharma, S. (2024). Integrating Durability with Strength in the Seismic Design Framework of Reinforced Concrete Structures with and without Fiber Reinforcement. PhD Thesis, Indian Institute of Technology Gandhinagar, India (To appear).
- Shen, D., Liu, X., Zeng, X., Zhao, X., & Jiang, G. (2020). Effect of polypropylene plastic fibers length on cracking resistance of high-performance concrete at early age. *Construction and Building Materials*. <https://doi.org/10.1016/j.conbuildmat.2019.117874>
- Shin, H. O., Yoo, D. Y., Lee, J. H., Lee, S. H., & Yoon, Y. S. (2019). Optimized mix design for 180 MPa ultra-high-strength concrete. *Journal of Materials Research and Technology*, 8(5), 4182–4197. <https://doi.org/10.1016/j.jmrt.2019.07.027>
- Smarzewski, P. (2019). Influence of basalt-polypropylene fibres on fracture properties of high-performance concrete. *Composite Structures*, 209, 23–33. <https://doi.org/10.1016/j.compstruct.2018.10.070>
- Sohail, M. G., Wang, B., Jain, A., Kahraman, R., Ozerkan, N. G., Gencturk, B., Dawood, M., & Belarbi, A. (2018). Advancements in concrete Mix designs: High-performance and ultrahigh-performance concretes from 1970 to 2016. *Journal of Materials in Civil Engineering*. [https://doi.org/10.1061/\(ASCE\)MT.1943-5533.0002144](https://doi.org/10.1061/(ASCE)MT.1943-5533.0002144)
- SP 228. (2005). Seventh international symposium on the utilization of high-strength/high-performance concrete. *ACI Committee*, 363, 79–80.
- Tan, K., & Zhu, J. (2017). Influences of steam and autoclave curing on the strength and chloride permeability of high strength concrete. *Materials and Structures*. <https://doi.org/10.1617/s11527-016-0913-6>
- Van, V. T. A., Röbber, C., Bui, D. D., & Ludwig, H. M. (2014). Rice husk ash as both pozzolanic admixture and internal curing agent in ultra-high-performance concrete. *Cement and Concrete Composites*, 53, 270–278. <https://doi.org/10.1016/j.cemconcomp.2014.07.015>
- Xu, L., Wu, F., Chi, Y., Cheng, P., Zeng, Y., & Chen, Q. (2019). Effects of coarse aggregate and steel fibre contents on mechanical properties of high-performance concrete. *Construction and Building Materials*, 206, 97–110. <https://doi.org/10.1016/j.conbuildmat.2019.01.190>
- Yew, M. K., Mahmud, H. B., Ang, B. C., & Yew, M. C. (2015). Influence of different types of polypropylene fibre on the mechanical properties of high-strength oil palm shell lightweight concrete. *Construction and Building Materials*, 90, 36–43. <https://doi.org/10.1016/j.conbuildmat.2015.04.024>
- Zhang, M. H., & Islam, J. (2012). Use of nano-silica to reduce setting time and increase early strength of concretes with high volumes of fly ash or slag. *Construction and Building Materials*, 29, 573–580. <https://doi.org/10.1016/j.conbuildmat.2011.11.013>
- Zhang, P., Wan, J., Wang, K., & Li, Q. (2017). Influence of Nano-SiO<sub>2</sub> on properties of fresh and hardened high performance concrete: A state-of-the-art review. *Construction and Building Materials*, 148, 648–658. <https://doi.org/10.1016/j.conbuildmat.2017.05.059>
- Zhou, F. P., Lydon, F. D., & Barr, B. I. G. (1995). Effect of coarse aggregate on elastic modulus and compressive strength of high-performance concrete. *Cement and Concrete Research*, 25(1), 177–186. [https://doi.org/10.1016/0008-8846\(94\)00125-1](https://doi.org/10.1016/0008-8846(94)00125-1)

## Publisher's Note

Springer Nature remains neutral with regard to jurisdictional claims in published maps and institutional affiliations.

**Dhiman Basu** Associate Professor, Department of Civil Engineering, Indian Institute of Technology Gandhinagar, India.

**Sheikh Mayesser Mushtaq** Formerly Research Associate, Department of Civil Engineering, Indian Institute of Technology Gandhinagar, India.

**Shivani Sharma** PhD Candidate, Department of Civil Engineering, Indian Institute of Technology Gandhinagar, India.

**Sandesh Tripathi** Formerly Graduate Student, Department of Civil Engineering, Indian Institute of Technology Gandhinagar, India.